The Detection of water ice in comet Hale-Bopp

Final
NCC 2-815

John K. Davies[1], **Ted L. Roush**[2,3], **Dale P. Cruikshank**[2], **Mary Jane Bartholomew**[2,4], **Thomas R. Geballe**[1], and **Tobias Owen**[5]

[1] Joint Astronomy Centre, 660 N A'ohoku Pl., Hilo, Hawaii 96720, USA. Tel 808 969 6524 Fax 808 961 6516 e-mail jkd@jach.hawaii.edu, tom@jach.hawaii.edu

[2] NASA Ames Research Center, Moffett Field, California, 94035-1000, USA. e-mail cruikshank@ssa1.arc.nasa.gov

[3] Department of Geosciences, San Francisco State University, San Francisco, California, 94132, USA. e-mail roush@barsoom.arc.nasa.gov

[4] Sterling Software, Redwood City, California, USA. e-mail mjb@ssa1.arc.nasa.gov

[5] Institute for Astronomy, 2680 Woodlawn Dr, Honolulu, Hawaii, USA. e-mail owen@uhifa.ifa.hawaii.ed

.....

Revision of 7-Nov-1996

.. Pages

4 Figures

1 Table

Keywords Comets, Composition; Infrared Observations; Spectroscopy.

Running Head Water Ice In Comet Hale-Bopp

Address for correspondence John Davies, Joint Astronomy Centre, 660 N A'ohoku Pl., Hilo, Hawaii 96720, USA. Tel 808 969 6524 Fax 808 961 6516 e-mail JKD@jach.hawaii.edu.

Abstract. We present spectra of Comet Hale-Bopp (C/1995 01) covering the range 1.4-2.5 μm that were recorded when the comet was 7 AU from the Sun. These show broad absorption features at 1.5 and 2.05 μm. We show that some, but not all, of this absorption could be matched by an intimate mixture of water ice and a low albedo material such as carbon on the nucleus. However we recognise that it is more likely that the ice features are produced by scattering from icy grains in the coma. The absence of absorption at 1.65 μm suggests that this ice is probably in the amorphous state. An unidentified additional component may be required to account for the downward slope at the longwavelength end of the spectrum.

1 Introduction

Although water is a major constituent of comets and has been detected in the gaseous phase a number of times (eg. see the review by Mumma *et al.*, 1993) the detection of solid phase water in comets has proven elusive. Direct observations of comet nuclei are usually prevented by their optically thick comae, and comets at large heliocentric distances, where the comae maybe thin or absent, are usually too faint for spectroscopic studies in the near-infrared (JHKL: 1.2-3.6 μm) regions where water ice is most readily detected.

Water ice is not however expected to be confined to the surface of cometary nuclei. As gas sublimes from the nucleus of an active comet grains are ejected at velocities of a few hundred m sec^{-1} to 1-2 km sec^{-1}. If volatile icy grains are ejected in sufficient quantity they may form an icy grain halo that is detectable spectroscopically before the individual grains evaporate. The rate of evaporation of these icy grains depends upon the heliocentric distance at the time of ejection. Energy balance calculations (Hanner 1981) show that unless icy grains are very pure, they cannot survive within about 2.5 AU of the Sun, precisely the region where comets usually brighten sufficiently to be observed easily. Only in the case of comets which are bright at large heliocentric distances is ice likely to be detectable, but such opportunities are rare. One possible detection of ice was reported in comet Cernis (Hanner 1984) where an absorption feature at 2.9-3.0 μm was deduced using CVF spectroscopy at three wavelengths, one in the ice band and two outside it. Campins *et al.* (1983) reported the detection of an absorption feature at 3.25 μm in comet Bowell which they attributed to a halo of icy grains around this comet, a possibility supported by A'Hearn *et al.* (1984) who reported that the OH production rate in Comet Bowell reached a maximum value beyond 4 AU at which time it was 10 times the rate recorded at perihelion. This surge in OH production was attributed to the sublimation of icy grains in the coma while the comet was still approaching the Sun.

However, despite these two pieces of evidence for icy grains in Comet Bowell Campins et al (1982) did not detect absorptions in the 1.25-2.3μm region which might have been expected from icy grains. To investigate this they investigated the scattering properties of various grain sizes via Mie scattering calculations and concluded that the best fit to their data was for particles with radii in the range 10μm and albedoes of about 5Such grains would be very dark for pure water ice but Clark (1981) has shown that even small amounts of dark material. eg soot, can dramatically darken icy surfaces until they have albedoes close to that of the dark contaminant. Campins et al (1982) thus proposed that the icy grain halo in comets at large heliocentic distances comprised a volatile matrix of water ice paticles in which were embedded dust grains which lowered the albedo to the order of 5

Comet Hale-Bopp was discovered on 1995 July 23 (*IAUC 6187*), at which time it was at a heliocentric distance of 7.4 AU and a geocentric distance of 6.4 AU. It was soon realised that the comet was unusually bright for an object at such a large heliocentric distance. Jets were observed in late 1995 by a number of observers. Sekanina (1996) has discussed the outburst history of comet Hale-Bopp and has compared its performance to other comets at large heliocentric distances. Jewitt *et al.* (1996) and Biver *et al.* (1996) detected emission from the CO which was presumably driving the production of the coma. In this paper we present near infrared spectroscopy during early September 1995, when the comet was 7 AU from the Sun, and report the detection of shallow absorption bands at 1.5 and 2.05 μm, which we attribute to H_2O ice.

2 Observations

Comet Hale-Bopp was observed on five nights between UT 1995 September 4 and September 9 using the cooled grating array spectrometer CGS4 of the United Kingdom Infrared

Telescope (UKIRT). CGS4 was equipped with its 75 line per mm grating and its short focal length camera, giving a pixel size of approximately 1.23 by 1.23 arc sec. The slit length was 90 arc sec. On some nights observations were made with a 1 pixel wide slit and on others a 2 pixel wide slit was used, see Table 1. The spectra generally were sampled three times per resolution element, and the detector was stepped over two pixels to ensure full spectral coverage in the presence of any bad pixels. The slit was oriented N-S during the observations which, since the tail position angle at the time was 86 degrees, placed the slit almost perpendicular to the Sun vector. Object-sky pairs of observations were made with the telescope being nodded along the slit between observations. The amplitude of this nod varied between 25 rows (approx 30 arc sec) and 10 rows (approx 12 arc sec) on different nights. The object and sky frames were differenced and the differences co-added to form a final frame containing two sky-subtracted comet spectra. On-chip single exposure times varied from 12 to 20 seconds in the J,H and K bands and 0.4s in the L band.

Comparison spectra were taken at airmasses that matched those of the comet and were used for removal of telluric features from, and flux calibration of, the comet spectrum. In the case of the data from September 4, for which the comparison star (CMC314447, V=9.04) was of spectral type A0, the final comet spectrum was divided by the mean stellar spectrum and the result was multiplied by a blackbody of temperature 9850K, the effective temperature of a star of that spectral type. We note that A0 stars have strong Brackett gamma absorption which, when the star is used for atmospheric cancellation, manifests itself as a spurious emission feature at 2.166 μm; this can be seen in the lower spectrum of Fig 1. The same procedure was used for the remaining nights using the calibration star BS6836 for which the bright star catalogue gives V=6.4 and spectral type G0V. Assuming the colours given by Johnson (1966) we used J=5.37 and K=5.05 for BS6836. Wavelength calibration was by reference to an argon emission lamp spectrum taken at the appropriate grating position each

night.

Details of the observations are given in Table I and the extracted spectra for each night are shown as Fig 1. In the case of the H band spectra, for which the spectra extracted from the two different nod positions showed some differences in shape, both spectra are shown (1a,b) For the remainder we show the average of the spectra extracted from the two nod positions as 1c-1f.

The optics of CGS4 produce a curvature of the spectrum across the detector array which must be removed before extracting spectra from specific rows of the array. The curvature is first determined by examining the spectrum of a point source, in this case the standard star. The images containing both the standard star and the comet are then rebinned to remove the effects of spectral curvature using routines in the Starlink Figaro reduction package. In all the images it was clear that strong continuum emission from the comet extended over several rows and the nodding along the slit may not have been sufficient to clear the coma completely. Examination of the spatial information provided along the slit showed that although the flux from from the comet was assymetric, falling away more rapidly to the south, it was fairly sharply peaked and so in each spectrum, irrespective of the distance nodded, only the central five rows were extracted. This corresponds to approximately the full width at half maximum of the cometary signal. With the 1.23 arc second pixel size and a one pixel wide slit, the extracted rows are equivalent to a retangular 1.23 by 6.2 arc second aperture which corresponds to a projected area of 5700 by 28500km at the distance of the comet. In order to provide an absolute value of the flux from the comet on each date, for each spectrum we present the flux at the centre of the standard JHKL filter passbands which was obtained by extracting from the flux calibrated spectra the average flux from a spectral region 0.04 μm wide centered on the nominal filter central wavelength (1.25, 1.65, 2.2 and

QQ μm respectively). These fluxes are are presented in Table 1 where it should be noted that not all are for the same effective aperture, since the slit width used was not the same for each observation, and fewer rows were extracted from the L spectrum to minimise the background noise.

Throughout the observations the comet was passing through the galactic plane close to the galactic centre and as a consequence other stars occasionally passed through the slit. Where these seemed likely to contaminate the spectra, individual object-sky pairs were removed from the final dataset before extracting the spectra.

3 The Composite Spectrum of Comet Hale Bopp.

Since the spectral features of interest are broad, and lie close to the edge of atmospheric windows, various wavelength settings were used in order to define the adjacent regions of continuum as accurately as possible. To improve the overall signal to noise ratio, all the spectra were combined to produce a single composite spectrum. The original flux calibrated spectra were divided by the incident solar flux which was calculated from Smith and Gottlieb (1974). The three K band spectra taken on September 4, 5 and 9 were scaled to unity at a wavelength of 2.2 μm. The H band spectra were then scaled to the mean K band spectrum at 1.66 μm. Data points with negative or zero flux values, believed to be due to noisy pixels and cosmic ray events, were deleted from the files as physically unrealistic.

All the data were then resampled to a common set of wavelength values spanning the entire range observed. This was done using a Gaussian convolution with a FWHM of 0.0009 μm. This corresponds to 1.5 spectral channels for the nights with the highest spectral resolution and results in a slight smoothing of the overall spectrum. A weighted average was calculated

from the convolved results. In order to determine the weighting we evaluated the point-to-point scatter in the scaled reflectance values for each observation over a 0.1 μm range which best represented a neutral part of the spectrum. Regions of high telluric absorption and the region of the 1.5 and 2.05 μm absorptions were excluded. Based upon the standard deviation of the point-to-point scatter the spectra were given the weights listed in Table I. After calculating the average spectrum, data points with standard deviations greater than 0.15 were deleted from the spectrum.

The J band spectrum was featureless and had no wavelength overlap with the remainder of the spectra taken. It is not plotted here. The L band spectrum (also not plotted) was very weak and even after combining several rows and smoothing the result revealed only a vague impression of a broad absorption between 3.0 and 3.2 μm with some hint of continuum from 3.2-3.6 μm. From this we estimate the L band continuum flux density to have been of the order 1 x 10^{-16} Wm^{-2} in an aperture 1.2 by 4.8 arc sec oriented EW x NS.

The individual H and K spectra are shown in Fig 1 and the resulting composite 1.4-2.5 μm spectrum is shown in Fig 2. In both figures two broad absorption features can be seen centred at wavelengths of 1.5 and 2.05 μm. In addition the spectral reflectance drops steeply at the long wavelength edge. Believing these absorptions to be due to the presence of water ice, we have investigated by means of Hapke theory, whether they can be explained by material on the nucleus of the comet. Because of limitations in our modelling code, we do not address the issue of an icy grain halo in this paper although we recognise that the scattering by grains must contribute significantly to the observed flux since the reflected light at 2.2 μm from a 10km nucleus of albedo 0.04 would be only 8 x 10^{-19} $Wm^{-2}\mu m^{-1}$, only 0.1% of the flux observed.

4 Mathematical Modeling - Equations and Assumptions

4.1 Intimate Mixtures

Hapke (1981, 1986, 1993a, 1993b) has developed a series of equations, based on a two-stream approximation to the equations of radiative transfer. This approach provides the ability to calculate the reflectance of a particulate surface given assumptions or knowledge about its physical nature and the solid phases comprising it. Such mixtures are commonly referred to as intimate mixtures where individual components exist as separate grains that are in turn thoroughly mixed at the micrometer scale.

The bidirectional reflectance of a surface, at each wavelength (λ), can be expressed as

$$r(\lambda, i, e, g, \overline{w}, h, S(0)) = \frac{\overline{w}}{4\pi} \frac{\mu_o}{\mu_o + \mu} \{[1 + B(g)]P(g) + H(\mu)H(\mu_o) - 1\} \quad (1)$$

where i and e are the angles of incident and emergent light, respectively (μ_o=cos i and μ=cos e), g is the phase angle between i and e, $\overline{w}$ is the average single scattering albedo of the particles composing the surface, h and S(0) are related to the width and amplitude of B(g) (the opposition surge) that is due to the microstructure of the surface (e.g., porosity, particle size distribution, and compaction rate with depth), P(g) is the the average particle phase function, and H(μ_o) and H(μ) are Chandrasekhar's (1960) H-functions. In all the models discussed below we assume an opposition effect that is is similar to that of other icy surfaces (i.e. h=0.05), an isotropic phase function (i.e. P(g)=1), and no internal scattering within the particles. The average single scattering albedo is related to the particles' relative mass fractions, solid densities, and wavelength dependent volume absorption coefficients (α)

(Hapke 1981, equation 17). The absorption coefficient is related to the imaginary index of refraction (k) through the dispersion relation ($\alpha = 4\pi k/\lambda$). See Roush *et al.* (1990, 1996), Roush (1994), and Cruikshank *et al.* (1996) for further details regarding the modeling.

Because absolute albedo information cannot be deduced from the observational data, due to the lack of knowledge of the diameter of the comet, both the observational data and the calculated spectra of the resulting mixtures are normalized by scaling them to a value of 1.0 at a wavelength of 1.73 μm for comparison purposes.

4.2 Spatial Mixtures

Spatial mixtures represent a surface having distinctive albedo regions present on a scale smaller than the spatial resolution of the observations. These are modeled by a linear combination of the reflectances of each region weighted by its spatial extent. The total reflectance of the surface (R_T) is expressed mathematically as

$$R_T = A*R_A + B*R_B + \cdots N*R_N \tag{2}$$

where A, B, and N are the spatial coverage and R_A, R_B, and R_N represent the spatial coverage and reflectance (as calculated from equation 1) of each component, respectively.

4.3 Optical Constants

The optical constants of water ice and amorphous carbon were used to calculate the reflectances discussed below. Water ice was selected because it exhibits absorption features at the same wavelengths as the observational data and because it is expected to be present in comets. Amorphous carbon was selected because it is a low albedo, spectrally neutral material. The real and imaginary indices of refraction of hexagonal water ice at 100K (Roush,

1996) and amorphous carbon (Rouleau and Martin, 1991) were used since this corresponds closely to the expected black body temperature at the distance of the comet. These refractive indices were linearly convolved to the same spectral resolution as the observational data. As mentioned above, the reflectances are directly influenced by any changes associated with the optical constants used in a calculation. If the optical constants used in these calculations are revised or supplanted by newer more accurate values then the results and conclusions presented below will be affected accordingly.

5 Calculations and Comparisons to the Observational Data

5.1 Pure Ice

Fig 3 shows the resultant calculations for a variety of grain sizes of pure water ice and a comparison of these to the comet Hale-Bopp data. The grain sizes cover a range that produce absorption features spanning the strengths observed for comet Hale-Bopp. However, it should be noted that the two finer grain sizes may violate the assumption of Hapke theory that the particles' cross sectional areas are greater than the wavelength of the incident radiation ($\pi d/\lambda \gg 1$). The H_2O ice spectra in Fig 3 exhibit absorption features centered near 1.5- and 2.0 μm and the wing of a strong feature centered near 3 μm. It is readily apparent that a surface composed solely of water ice can roughly reproduce the water ice features seen in the comet Hale-Bopp spectrum at the shorter wavelengths but cannot reproduce the relative strength of the three bands. In particular the $3\mu m$ band is too strong relative to that expected from the model spectra. This suggests that some additional component or alternative mechanism gives rise to the extra absorption at wavelengths $\geq$2.2 μm.

5.2 Intimate Mixtures

Because water ice cannot simultaneously reproduce the relative strengths of the 1.5, 2.0, and wing of the 3 μm absorptions, only data lying between 1.4 and 2.2 μm were used to model the observational data. The model represented the surface as an intimate mixture of water ice and amorphous carbon and the fitting algorithm consisted of a downhill simplex approach (Press *et al.* 1989) that minimized the expression,

$$\chi^2 = \sum_{i=1}^{n} \frac{(r_o - r_c)^2}{{\sigma_o}^2} \tag{3}$$

where the sum is over wavelength, r_o and r_c are the observed and calculated reflectances, respectively, and σ_o is the standard deviation of the observed reflectance. This approach was used to determine the relative mass fraction and grain size for each component. Once the algorithm converged to a particular solution, the resulting parameters were used to calculate the scaled reflectance over the entire wavelength range of the observational data. In an attempt to avoid local mimima in the parameter space, the algorithm was initialized at several different locations; only two of the best solutions are illustrated in Fig 4.

Fig 4a shows the results of the spectrum fitting procedure for a homogenous surface composed of roughly one quarter water ice and three quarters amorphous carbon having grain diameters of 133 and 14 μm, respectively. The relative strengths of the 1.5 and 2.0 μm bands are reproduced well by the model, however, the absorption at longer wavelengths is not. We note a discrepancy between the model and the comet spectrum at 1.65 μm. At this wavelength a temperature-sensitive absorption band of crystalline ice occurs. The absorption is minimal for T $\geq$ 200K, and increases with decreasing temperature (Fink and Larson 1975). Amorphous ice at T=100K shows minimal absorption at this wavelength (Fink and Sill 1982). The model spectrum presented here shows absorption at 1.65 μm because the

optical constants used were derived from spectra of crystalline ice at 100K in which moderately strong absorption occurs at that wavelength. The absence of the absorption feature in the comet spectrum is therefore suggestive of the presence of amorphous ice.

The exothermic phase transition from amorphous to crystalline water ice occurs in the temperature range 125-150K (Mumma *et al.* 1993) and so amorphous ice might not be expected close to the surface of comets which have made one or more perihelion passages at distances less then a few AU. However, while comet Hale-Bopp is not new in the Oort sense, the detection of CO shows that some very volatile materials have been retained in the nucleus and are only now becoming manifest. Amorphous or cubic phases of water ice could also have survived and may now be being brought from within the comet by the jets observed in the visible. At present optical constants of these phases of water ice are not available at the wavelengths associated with the comet data presented here but when such data are available it may be that models using such values might provide a better correspondence to the observations. The alternative possibility that the ice is crystalline but at $T \geq 200K$ is highly improbable for a comet at 7 AU from the sun.

A particle size distribution was investigated by including an additional water ice component having a different grain size than the initial water ice component. A resultant solution is shown in Fig 4b. In this mixture, water ice occurs as two grain sizes, 133 μm and 27.7 mm that combined have greater abundance ($\approx$40%) while the amorphous carbon has a larger grain size 21 μm, but is less abundant than in the two component mixture. However, the spectral characteristics of the water ice with grain sizes of $\approx$28 mm would closely resemble those of amorphous carbon, i.e. it would have a low albedo and be spectrally neutral over the entire wavelength region investigated here. Nevertheless, the resulting mixture reproduces the 1.5 and 2.0 μm band strengths well, but again cannot produce the long wavelength

absorption.

5.3 Spatial Mixtures

The ability of spatial mixtures of water ice and amorphous carbon to describe the observations were also investigated. Because amorphous carbon is strongly absorbing its calculated reflectance is independent of grain size (at least over the grain size range that remains consistent with the assumptions of Hapke scattering models). The reflectances were calculated for pure water ice having grain diameters of 5-, 10-, 50-, 100-, 500-, and 1000 μm. A commercially available curve fitting routine (*SigmaPlot*) was used to determine the relative abundances of mixtures of amorphous carbon and water ice. This software relies on a Marquardt-Levenberg algorithm. Like the intimate mixtures discussed above, only the observational data lying between 1.44 and about 2.2 μm that were scaled to 1 at 1.73 μm were used in the fitting procedure. Once a solution was determined, the derived relative abundances were used to calculate a spectrum over the entire wavelength range of the observational data and equation 3 was used to calculate χ^2.

The best fitting spatial mixtures, shown in Figs 4c and 4d, resulted from the two finest grain diameters of water ice and yielded similar relative abundances. Both consist of 99% amorphous carbon and 1% water ice. The χ^2 values were very similar to the best fit intimate mixtures.

6 Conclusions

Due to limitations in out modelling code we have restricted this analysis to intimate and spatial mixtures on a solid surface although we recognise that in reality reflection from the

nucleus is not the major contributor to the flux recieved from the comet even at this large heliocentic distance. Least-squares fitting proceedures that model the reflection of incident sunlight by a particulate surface suggest that water ice can reproduce the relative strengths of the 1.5 and 2.0 μm absorptions observed in comet Hale-Bopp's spectrum. A range of solutions, involving one or two particle sizes for water ice, intimately mixed with a low albedo neutral color material such as amorphous carbon, suggest that the grain size of water ice responsible for the observed band strengths is $\approx$100 μm and constitutes a relative mass fraction of roughly 15-25%. Spatial mixtures of amorphous carbon and water ice favour a surface dominated by amorphous carbon (99%) with minor areas of fine grained water ice (1%). Spatial mixtures and intimate mixtures provide solutions that, based on the quality of fit to the observational data, are comparable. However, none of the mixtures can reproduce the observed absorption at wavelengths $\geq$2.2 μm. This suggests that either (1) another material is present that gives rise to the additional absorption but lacks other distinctive spectral features at these wavelengths; or (2) some other mechanism is giving rise to the additional absorption, e.g., absorption due to icy grains present in the coma of comet Hale-Bopp. Scattering from particles in an icy grain halo may account for the discrepancy at the longer wavelengths. The presence of a large number of neutral scattering grains in the coma may also have the effect of diluting the absorption features seen in a relatively large beam. This would reduce the amount of neutral material required in each grain to match the relatively shallow features seen in the data. We are presently working on modeling code to explore scattering models. Although optical constants at the relevant wavelengths for amorphous ice are not presently available, we are attempting to obtain such data in order to explore the possibility that the absorptions in comet Hale Bopp are due to ice in the vitreous phase.

6.1 Acknowledgements

We thank the staff of UKIRT for its support of these observations. Some of this research is supported by Planetary Geology and Geophysics program via NAGW-2212 and RTOP 151-01-60-44.

UKIRT is operated by the Joint Astronomy Centre on behalf of the Particle Physics and Astronomy Research Council.

7 References

A'Hearn, M.F., D.F. Schleicher, P.D. Feldman, R.L. Millis, and D.T. Thompson (1984) Comet Bowell 1980b, *Astron. J.* **89,** 579-591.

Biver, N, Rauer,H.,Despois,D., Moreno, R.,Paubert, G.,Bockelee-Morvan, D., Colom,P., Crovisier,J., Gerard,E., Jorda,L. (1996) Huge outgassing of carbon monoxide from comet Hale-Bopp at large heliocentric distance. *Nature* **380 (6750)** 137-139

Campins, H Rieke, G.H., Lebofsky, M.J. and Lebofsky, L.A. (1982) A Search for Frosts in Comet Bowell (1980b). *Astron J.*, **87** 1867-1873

Campins, H Rieke, G.H. and Lebofsky, M.J. (1983) Ice in Comet Bowell. *Nature* **302** 405-406

Chandrasekhar, S. (1960) *Radiative Transfer*, Dover, New York, 393pp.

Clark, Roger N. (1981) *JGR*, **86**, **B4**, 3074-3086

Cruikshank, D.P., T.L. Roush, J.M. Moore, M. Sykes, T.C. Owen, R.H. Brown, and K.A. Tryka (1996) *The Surfaces of Pluto and Charon*, in *Pluto and Charon*, edited by D.J. Tholen and A. Stern, University of Arizona Press, Tucson, Arizona, in press 1996.

Fink, U. and H. P. Larson (1975) Temperature dependence of the water-ice spectrum between 1 and 4 microns: Applications to Europa, Ganymede and Saturn's rings. *Icarus* **24** 411-420.

Fink, U. and G. T. Sill (1982) The infrared spectral properties of frozen volatiles. In Comets (L. Wilkening, ed.), pp. 164-202. Univ. of Arizona Press, Tucson.

Hanner, M.S. (1981) On the Detectability of Icy Grains in the Comae of Comets., *Icarus*, **47** 342-350

Hanner, M.S. (1981) Comet Cernis: Icy Grains at Last? *Ap J*, **277** L75-L78

Hapke, B.W. (1981) Bidirectional reflectance spectroscopy I. Theory, *J. Geophys. Res.*, **86**, 3039-3054.

Hapke, B.W. (1986) Bidirectional reflectance spectroscopy 4. The extinction coefficient and the opposition effect, *Icarus*, **67**, 264-280.

Hapke, B.W. (1993a) *Combined Theory of Reflectance and Emittance Spectroscopy*, in *Remote Geochemical Analysis: Elemental and Mineralogical Composition*, C.M. Pieters and P.A.J. Englert, Eds., Cambridge Univ. Press, New York, New York, pp. 31-42.

Hapke, B.W. (1993b) *Reflectance and Emittance Spectroscopy*, Cambridge Univ. Press, New York, New York, 359pp.

Jewitt, D., Senay, M. and Matthews, H.E. (1996) Observations of Carbon Monoxide in Comet P/Hale-Bopp. *Science* **271,** 1110-1113.

Johnson

Mumma, M. J., Weissman, P. R., and Stern, S. A. (1993). Comets and the origin of the solar system: Reading the Rosetta Stone. In *Protostars and Planets, III* (E. H. Levy and J. I. Lunine.eds) pp. 1177-1252. Univ. of Arizona Press, Tucson.

Press, W.H., B.P. Flannery, S.A. Teukolsky, and W.T. Vetterling (1989) *Numerical Reciepes. The Art of Scientific Programming,* Cambridge University Press, New York, New York, 702pp.

Rouleau, F. and P.G. Martin (1991) Shape and clustering effects on the optical properties of amorphous carbon *Astrophys. J.*, **377**, 526-540.

Roush, T.L. (1996) Near-IR (0.8-2.5 μm) optical constants of water ice at 100K (abstract), *Lunar Planet. Sci. Conf. XXVIII*, Lunar and Planetary Institute, Houston, TX, 1107-1108.

Roush, T.L. (1994) Charon: More than water ice? *Icarus*, **108**, 243-254

Roush, T.L., J.B. Pollack, F.C. Witteborn, J.D. Bregman, and J.P. Simpson (1990) Ice and minerals on Callisto: A reassessment of the reflectance spectra, *Icarus*, **86**, 355-382.

Roush, T.L., D.P. Cruikshank, J.B. Pollack, E.F. Young, and M.J. Bartholomew (1996) Near-infrared spectral geometric albedos of Charon and Pluto: Constraints on Charon's surface composition, *Icarus*, **119**, 214-218.

Sekanina, Z. (1996). Activity of Comet Hale-Bopp (1995 O1) beyond 6 AU from the Sun. *A and A* (submitted).

Smith, E.V.P. and D.M. Gottlieb (1974) Solar flux and its variations, *Space Sci. Rev.*, **16,** 771-802.

Date Sept	Slit width arcsec	Lambda Range μm	R $\lambda/\delta\lambda$	Sec z	Nod arcsec	Aperture arcsec	Flux at λ μm	Flux $Wm^{-2}\mu m^{-1}$	sp wt
4.3	2	1.85-2.51	450	1.65	30.7	2.48 * 6.2	2.2	$3.39 \pm 0.10 \times 10^{-15}$	1
4.3	2	1.32-1.98	320	1.76	30.7	2.48 * 6.2	1.65	$3.78 \pm 0.29 \times 10^{-15}$	1
5.2	1	1.84-2.50	850	1.57	12.3	1.24 * 6.2	2.2	$2.19 \pm 0.16 \times 10^{-15}$	3
6.2	1	1.01-1.36	450	1.58	12.3	1.24 * 6.2	1.23	$8.82 \pm 0.31 \times 10^{-15}$	0
7.2	1	1.57-2.23	750	1.58	12.3	1.24 * 6.2	2.2	$2.23 \pm 0.19 \times 10^{-15}$	3
9.2	1	1.64-2.30	770	1.64	18.4	1.24 * 6.2	2.2	$2.64 \pm 0.29 \times 10^{-15}$	5
9.3	1	3.01-3.69	1300	1.56	18.4	1.24 * 4.9	QQ	$3.0 \pm 1.0 \times 10^{-16}$	0

Table 1: Details of the Observations taken

8 Figure Captions

Figure 1 The six separate observations used to determine comet Hale-Bopp's composite spectrum. The spectra in a and b were scaled to the mean K-band spectrum at 1.66 μm. The spectra in c-f were scaled to 1.0 at 2.2 μm.

Figure 2. The composite spectrum of Hale-Bopp (top curve) and associated standard deviations (bottom curve). The data have been resampled to common wavelength scale, points with standard deviations greater than 0.15 have been deleted, and rescaled to 1.0 at 1.73 μm.

Figure 3. Comet Hale-Bopp data (heavy solid line) compared to the reflectance calculated for water ice having grain diameters of 1 μm (dashed line), 5 μm (dotted line), and 10μm (thin solid line).

Figure 4. Comet Hale-Bopp data (solid lines) compared to (a) the reflectance calculated for a two component intimate mixture of water ice and amorphous carbon. (b) a three component intimate mixture containing two particle sizes of water ice. (c) a two component spatial mixture of amorphous carbon and 5 μm diameter water ice, and (d) a two component spatial mixture of amorphous carbon and 10 μm diameter water ice.

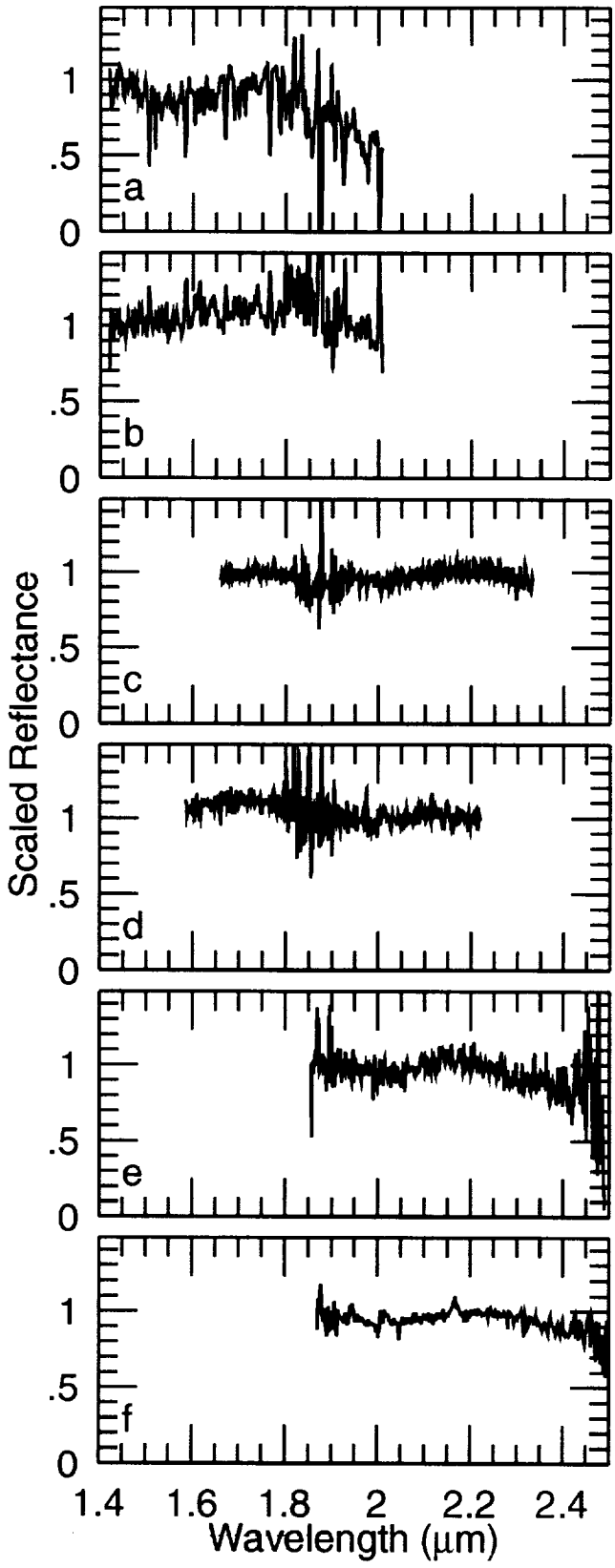

Davies et al. Figure 1

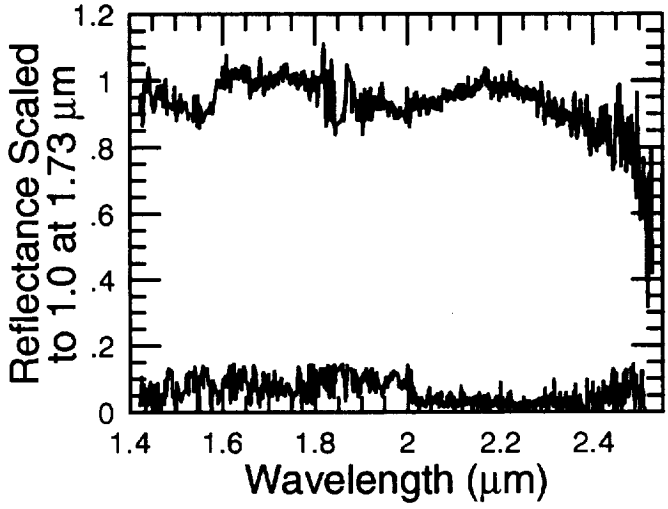

Davies et al. Figure 2

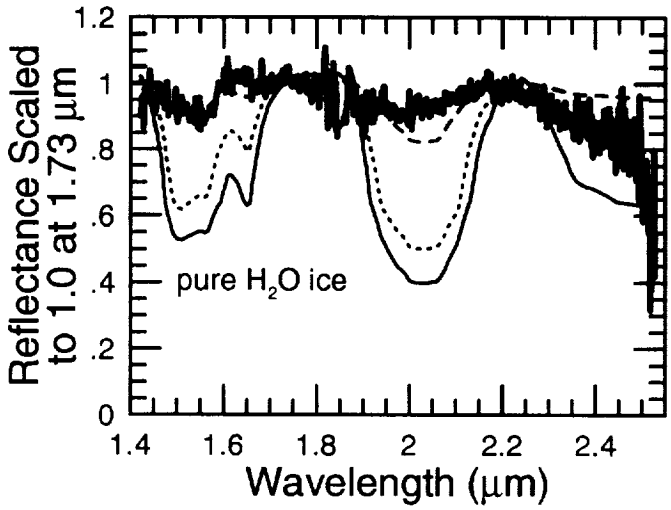

Davies et al. Figure 3

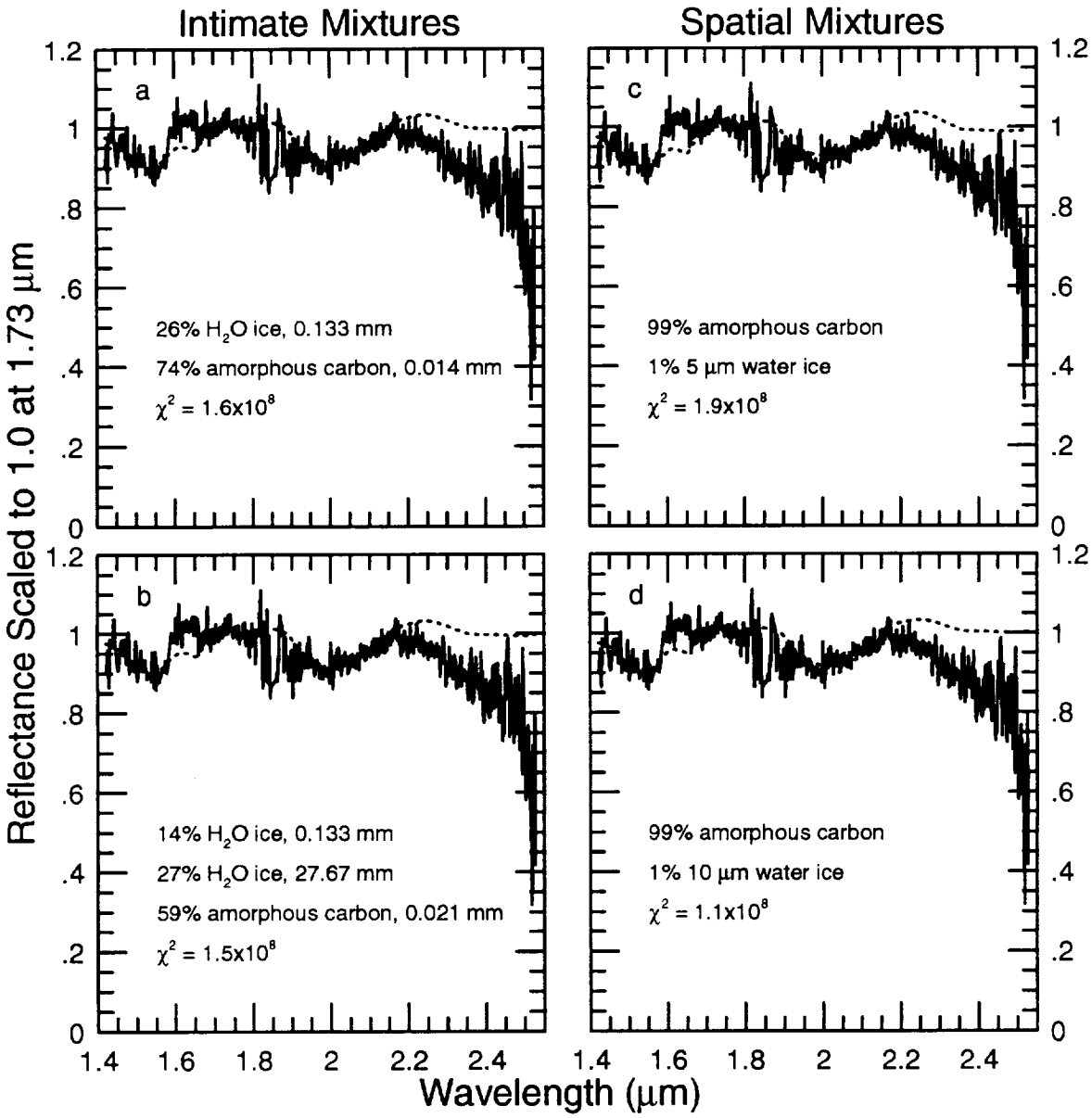

Davies et al. Figure 4